J MATER SCI 41 (2006) 1109–1121

Structural characteristics and mechanical behaviour of beard hair

S. M. THOZHUR, A. D. CROCOMBE, P. A. SMITH*
School of Engineering, University of Surrey, Surrey, UK
E-mail: p.smith@surrey.ac.uk

K. COWLEY, N. MULLIER
Gillette Management Inc., Reading, UK

Published online: 4 February 2006

The structural characteristics of beard hair have been analysed using optical microscopy, scanning electron microscopy and atomic force microscopy. The cross-sectional profile of beard hair is found to be broadly elliptical. The three main morphological features cited in previous literature for scalp hair, namely the cuticles, cortex and medulla were observed. A novel and efficient method has been developed in order to characterise the cross sectional area of an elliptical hair accurately. Quantitative data are presented for the variation of average cross-sectional area across different facial sites (cheek, chin and neck) for three different subjects. Tensile tests have been conducted on a variety of specimens to study the tensile stress-strain behaviour of beard hair in both wet and dry state at a range of cross-head speeds. Application of the area characterisation method significantly reduced the scatter in the mechanical data. The Young's modulus and yield stress values of beard hair are affected significantly by the presence of moisture but only to a limited extent by the strain rate. Repeat tensile tests have been conducted on beard hair samples which were kept in storage for nine months. A drop in the Young's modulus of up to 30% has been observed indicating an "ageing" effect (due to prolonged storage) on the properties of the hair.

1. Introduction

Understanding the behaviour of hair has been a subject of interest in the cosmetics industry for several decades. In order to manufacture high quality cosmetic products for use on hair, it is necessary to acquire a good understanding of the hair structure and its behaviour under load. Studies on the physiology and structure of scalp hair by several authors [1–6], have shown that the microstructure broadly consists of three distinct zones, namely the cortex, the medulla and the cuticle. The cortex constitutes the bulk of the hair and is the part which contributes mainly to the tensile strength [7]. Thus hair cannot be considered as a homogeneous and isotropic material and predicting the behaviour of hair as an engineering material would involve giving due consideration to its biological features. The diameters of beard or scalp hair vary from person to person and even within the same person; they also vary with factors such as age and race. Thus assigning an average value for the diameter is quite difficult. Studies suggest that the diameter of beard hair is nearly twice that of scalp hair [8].

Much work has been carried out to understand the behaviour of scalp hair under tension and efforts have also been made to understand behaviour under other modes of loading such as torsion, bending and friction. In the case of scalp hair, factors such as age, race, moisture conditions, site (on the body) and testing conditions (such as strain rate) have been reported to influence the behaviour. For example, the Young's modulus of scalp hair in the Hookean region has been reported to reduce by a factor of 3 from a dry to wet state while its torsional stiffness has been reported to vary by a factor of 10 from a dry to wet state, [9] as quoted by [7].

As a part of understanding the constitutive behaviour of hair, attempts have been made to develop mechanical and

*Author to whom all correspondence should be addressed.
0022-2461
DOI: 10.1007/s10853-005-3648-2

finite element models. Feughelman [10], as quoted in [11], proposed a mechanical model for hair where he suggested a two phase structure constituted by the α-helices in the microfibrils and the matrices in which they are embedded to explain the tensile behaviour. This approach was developed by Sakai *et al*. [11] who studied the mechanical properties of human hair fibre in their attempt to build a universal structural model for human hair to understand its mechanical and permeation properties. They suggested a "two part/two state" model, wherein hair is segregated into two structural parts (each part being comprised of a set of morphological features), both of which exhibit two different states at certain temperature conditions (hence the term two part/two state). There have been other models proposed for explaining the hair behaviour in tension such as the series zone model [12] to explain the yield and post yield regions in the tensile behaviour and the extended two phase model [13] to explain the behaviour in the post yield region.

Most of the authors referred to above have worked on scalp hair. Although a few authors have reported results on the mechanical behaviour of beard hair [8, 14], limited consideration has been given to aspects such as the effect of facial site, subject age and accuracy of the cross-sectional area characterisation. Also, there is a lack of sufficient published literature which combines the effects of factors such as moisture and strain rate on the tensile properties of human beard hair. The present work is aimed at gaining a better understanding of the mechanical properties of beard hair by giving consideration to factors such as subject age, facial site, moisture and strain rate. A better understanding of the mechanical behaviour of hair will assist in development of the finite-element-based simulations to predict deformation and fracture of hair during cutting operations.

This paper contains five sections. The first section describes the experimental methods adopted for the microstructural and mechanical characterisation of beard hair. The next section presents the microstructural observations. The observations made using optical microscopy, scanning electron microscopy and atomic force microscopy have been presented. This leads to a description of the method developed for cross-sectional area measurement of beard hair and its validation before data relating to the variation of cross-sectional area over the entire range of samples selected for study are presented. Next, the results from mechanical testing are given. Following this, a summary of the data from the tensile tests has been included along with a discussion on the effects of strain rate, moisture and repeatability. In the final section, concluding remarks are made. The biological aspect of the paper has been kept relatively simple since its main purpose is to support the engineering aspect of the study and give a very brief insight to a reader coming from a non-biological background about the relevant biological aspects of hair.

2. Experimental method

2.1. Samples

Samples of facial hair were obtained from three different caucasian males of ages 61 (designated as subject A), 53 (designated as subject B) and 39 (designated as subject C) respectively. Samples were harvested from three different facial sites, namely cheek, chin and neck. The samples were tested initially within a few days following harvesting.

2.2. Microstructural characterisation

2.2.1. Sectioning and light microscopy

Optical microscopy was carried out on cross sections of a range of beard hair samples, using a Zeiss Axiophot optical microscope. The specimens were prepared by mounting the beard hair in a methacrylate resin which was cured at 70°C for 24 h. The mould configuration is shown schematically in Fig. 1.

Special care was taken to ensure that the hair filament was pre-tensioned slightly and held straight inside the mould. The resin block containing the hair was then removed from the mould and the specimen mounted in the resin was subsequently polished to a 0.25 μm finish before examination using optical microscopy.

2.2.2. Scanning electron microscopy

Scanning electron microscopy was performed using Hitachi S-4000 scanning electron microscope (SEM). The samples were sputter coated with gold prior to examination, in order to prevent charging and the images were taken at 5 kV. Initially, as received samples were mounted longitudinally on stubs using a nail varnish, in order to study the cuticle structure on the surface. Scanning electron microscopy was also performed on the mounted beard hair cross-sections to examine the cortex and medulla regions in more detail.

2.2.3. Atomic force microscopy

Atomic force microscopy was perfomed on samples using Nanoscope III atomic force microscope in order to examine the cuticles in more detail. The specimen preparation procedure followed was reasonably simple with the hair samples just being bonded onto stubs. Images were taken in tapping mode.

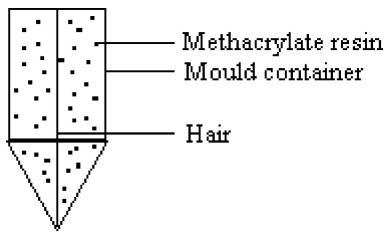

Figure 1 Mould configuration used for preparing hair cross-sections.

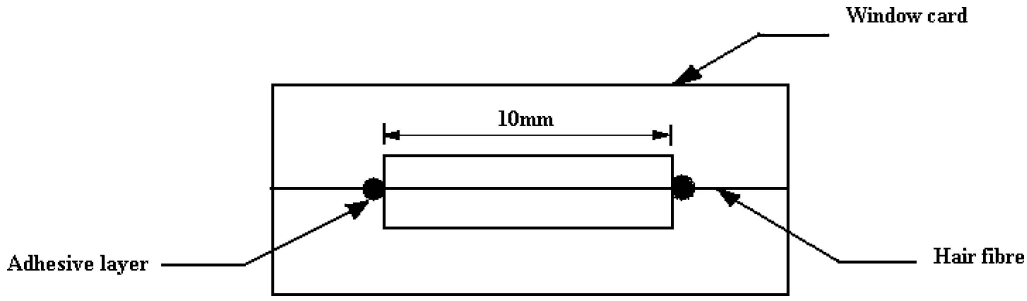

Figure 2 Schematic diagramme of window card with a hair mounted.

2.3. Mechanical characterisation

2.3.1. Sample preparation

The specimens for tensile testing were prepared by adopting the method suggested by ASTM for single fibre testing (ASTM D 3379). Hair samples were bonded onto window cards of 10 mm gauge length using a commercial super glue. A schematic of the window card with a hair mounted on it is shown in Fig. 2. The cross-sectional dimensions were measured at four different points along the length of the hair and at three different specimen plane orientations relative to the datum. This was necessary in order to determine the cross-sectional area using the method that will be discussed in a later section. The "as received" beard hair samples were only slightly longer than the gauge length. Thus it can be said that for every sample, the entire section was tested in tension.

2.3.2. Mechanical testing

The window cards were gripped in an Instron 1175 mechanical testing machine using pneumatic grips working at 50 psi (0.342 MPa). The sides of the window card were cut to enable the hair to take the entire load. A 100 N load cell was used. The samples were tested at crosshead speeds of 0.05, 5 and 50 mm min^{-1}. The strain was evaluated from the crosshead movement. To confirm the accuracy of the strain measurement based on the crosshead movement, a minute drop of Tip-ex® was applied to a hair, and the tensile test was captured using video microscopy. The video was then replayed and the strain on the hair as deduced from the extension of the Tip-ex drop at different time intervals was correlated with the corresponding strain value derived from the crosshead movement. The correlation was found to be reasonable and thus it was decided that the strain measurements derived from the crosshead movement were acceptable.

Tests were performed on both dry and wet beard hair. Specimens to be tested "wet" were soaked in water for 30 min before testing. For this, a moist piece of cotton wool was carefully draped over the exposed portion of hair mounted on a window card. A correction factor of 1.11 was used to adjust the area of dry hair to account for the swelling of hair in water. To derive the correction factor, the dry area of a point in a sample was evaluated in the usual way and the sample was moistened for a period of 30 min. Following wetting, the increase in transverse dimension at one plane of observation was noted and the percentage increase was applied to the transverse dimensions at other orientations assuming an isotropic swelling. The new swollen area was then compared with the old area. The process was repeated over several samples and the average increase in area was used to arrive at the correction factor.

In order to assess the effect of ageing on the mechanical properties of beard hair, tensile tests were repeated on samples taken from the cheek of subject 'C' which were stored for a period of nine months following removal from the donor. Ten samples were used, five each for wet and dry tests, at a crosshead speed of 5 mm min^{-1}. In the case of wet samples, it was found by re-examination, that the extent of swelling was similar to that observed in the fresh samples, and thus the same correction factor of 1.11 was applied to account for the increase in cross-sectional area of samples following wetting. Subsequent to testing, some of the fracture surfaces from specimens which exhibited gauge length failure were examined in the SEM.

3. Microstructural observations

3.1. Optical microscopy

Typical reflected light micrographs of beard hair cross-sections taken from each of the three facial sites (cheek, chin, neck) are shown in Fig. 3 for subjects A and C.

The optical micrographs suggest that the cross sectional shape of beard hair can be approximated as being elliptical. In some of these samples, the three main morphological features of hair can be identified clearly. For example, in Fig. 3c, the cuticle layer can be seen as a thin dark outer boundary. The cortex can be seen as a thick grey region and the medulla as the inner dark region. It is known from the literature, that the cortex plays the main role in the behaviour of hair in tension [15]. While the cuticles may play some role in bending [16], the cortex still dominates the behaviour. As seen from the figures, the cross-sectional dimensions vary from sample to sample. The major axis is in the range from 130 to 170 μm while the minor axis is in the range from 50 to 80 μm. More detail of the cuticle, cortex and medulla can be gained from the SEM observation in the next section.

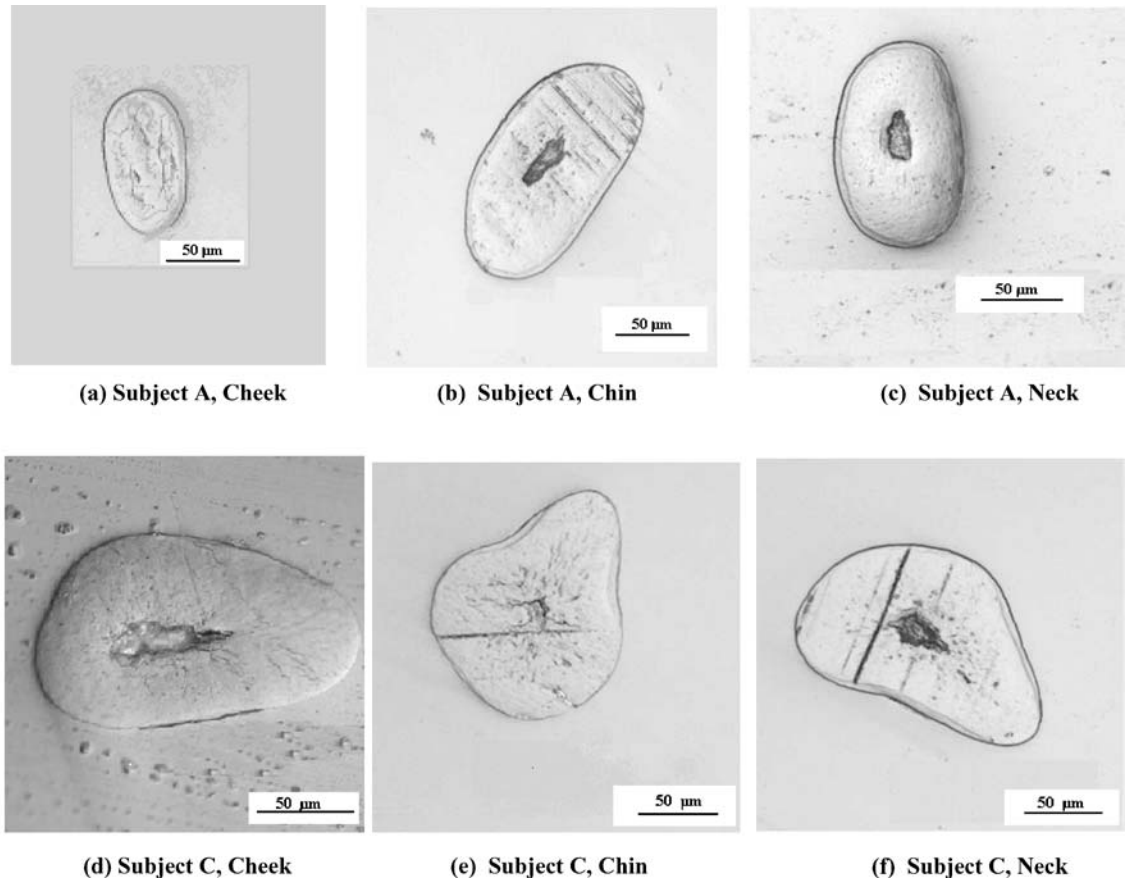

Figure 3 (a–f) Optical micrographs of beard hair cross-sections taken from different facial sites of subjects A and C.

3.2. Scanning electron microscopy

3.2.1. Cross-section

Fig. 4 shows an SEM photomicrograph of a beard hair specimen cross-section with the medulla as the micro-cracked structure in the centre. Previous studies indicate that the medulla consists of a cortex like framework of a spongy keratin substance and plays the role of empty space without participating as a load bearing member. It appears from the images that the medulla, which is giving a coarser appearance than the cortex, is relatively softer and less densely packed than the cortex.

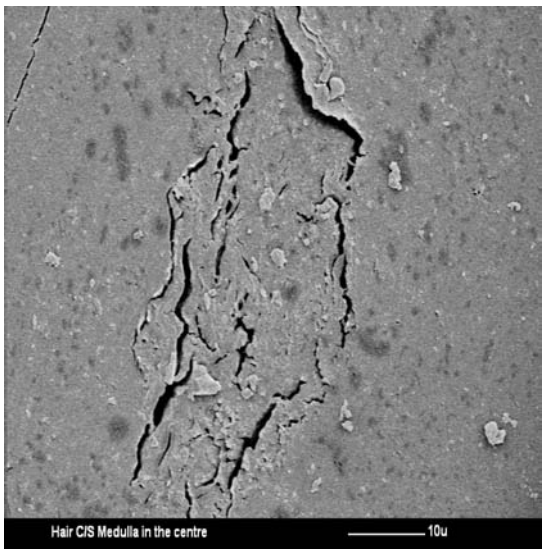

Figure 4 Scanning electron micrograph of a polished beard hair cross-section.

3.2.2. Surface morphology

A scanning electron micrograph of the surface structure of a beard hair sample is shown in Fig. 5. The cuticle structure shown in the figure is typical of those observed and it can be seen that the basic "roof tile" like arrangement of the cuticle cells are similar to that cited in the literature for scalp hair [1–6]. The thickness of a cuticle leaf appears to be around 0.5 μm. The number of cuticle layers in beard hair has been reported to be around 8 to 11 [8]. Since the number of cuticle layers in beard hair is larger than that in scalp hair, it may be that consideration needs to be given to the cuticles while modeling the constitutive behaviour of beard hair.

3.3. Atomic force microscopy

An atomic force micrograph of the surface structure of a beard hair sample is shown in Fig. 6. The 'roof tile' type cuticle structure is clearly seen in the micrograph. A section analysis performed along the imaged area

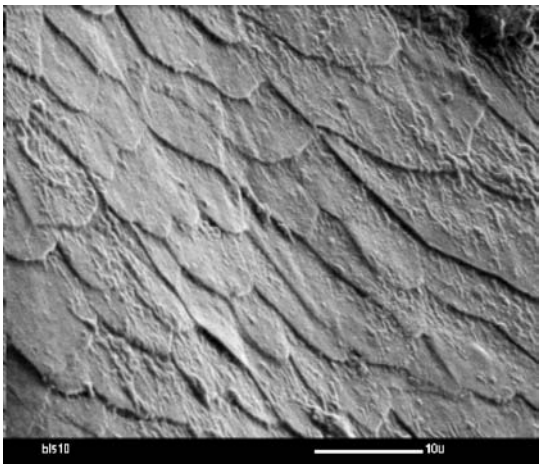

Figure 5 Scanning electron micrograph showing typical cuticle structure of beard hair.

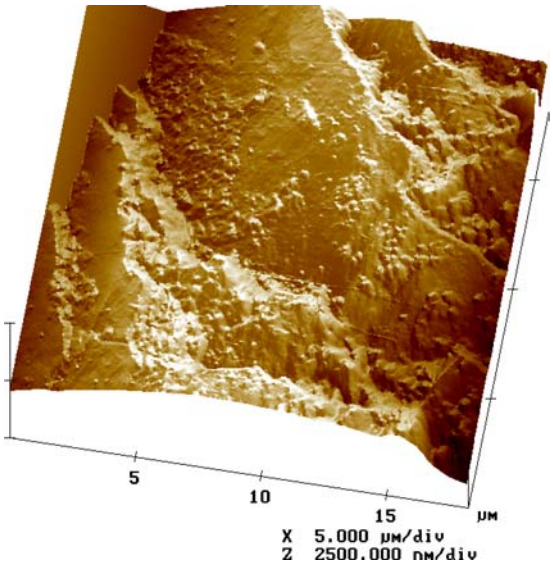

Figure 6 Micrograph showing image of a beard hair surface (cuticle cells) from atomic force microscopy.

suggested that the cuticle leaf thickness is about 0.5 to 1 μm which is consistent with the values cited in the literature for scalp hair. The cuticle layers appear to be quite rough and the ends are not as well profiled as they appear from scanning electron microscopy. However, since the resolution achieved in atomic force microscopy is much higher than that in scanning electron microscopy, minute damages caused by drying or rough handling would be more apparent in AFM.

4. Cross-sectional area measurement

4.1. Algorithm

Through light microscopy, it appeared that the cross-sections of a majority of the beard hair samples were roughly elliptical in shape. For an elliptical profile, it is obvious that taking transverse measurements at one or two different specimen plane orientations and averaging the results (assuming a circular cross section) would give an inaccurate measure of the cross sectional area. In order to avoid this problem, a suitable algorithm was developed that was used to predict the cross-sectional dimensions more accurately, whilst taking measurements at only a few angles of rotation of the specimen plane. The idea behind the approach is to theoretically link the transverse measurement of a section of an elliptical prism (and the corresponding orientation angle from a datum) to its major and minor axes and their offset from the same datum. The derivation of the relevant equations is presented in the appendix. In summary, for an elliptical prism, with major diameter 2a and minor diameter 2b where the major diameter is inclined at an angle β to the (horizontal) viewing plane as shown in Fig. 7, the following relationships can be obtained:

$$\Phi = \tan^{-1}\frac{(b\tan\beta)}{a}$$

$$\mathrm{OS}' = (b\sin\Phi\tan\beta + a\cos\Phi)\cos\beta$$

$$\beta = \beta' + \alpha$$

In these relationships, OS′ is half the apparent diameter measured by light microscopy at an inclination angle β. α is the unknown inclination of the major axis to the initial (datum) viewing plane, β' is the rotation from this initial position and Φ is the ellipse eccentric angle for the measurement point. Given the data for the measured transverse dimension at a point for several orientation angles, an Excel® spreadsheet is used to implement the

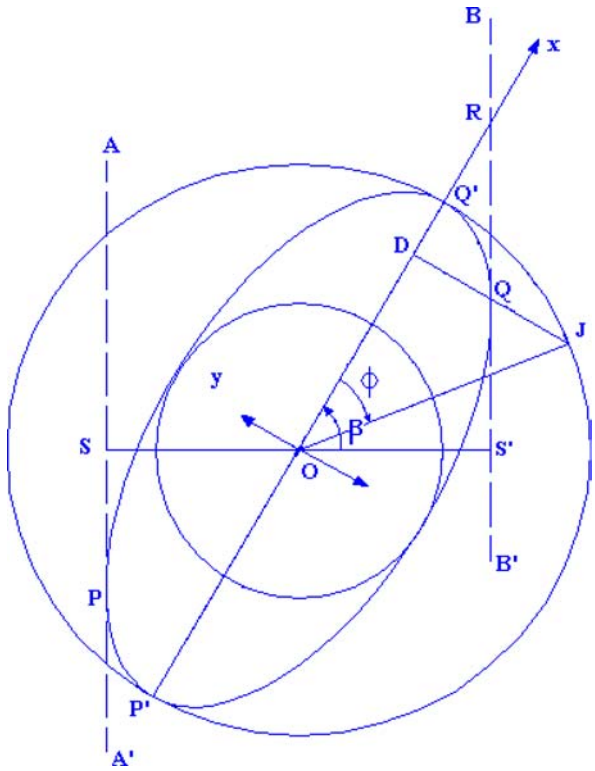

Figure 7 Geometric representation of hair assumed to be an elliptical prism being observed under a light microscope.

TABLE I Application of the Excel program to real ellipses of known dimensions

Ellipse configuration	Transverse measurements at different inclinations			Error in area from spreadsheet using two measurements at 0° and 90° (%)	Error in area from spreadsheet using three measurements at 0°, 45° and 90° (%)
	$\beta = 0$ (μm)	$\beta = 45$ (μm)	$\beta = 90$ (μm)		
$a = 80, b = 40, \alpha = 35$	138	82	114	22	0.9
$a = 50, b = 30, \alpha = 35$	88	61	76	12	0.5
$a = 50, b = 30, \alpha = 25$	94	65	70	10	0.8
$a = 50, b = 30, \alpha = 60$	71	64	93	10	0.1
$a = 50, b = 30, \alpha = 120$	72	99	91	9	3
$a = 50, b = 30, \alpha = 150$	92	99	72	10	3
$a = 50, b = 30, \alpha = 170$	98	88	61	2	0.3
$a = 50, b = 30, \alpha = 135$	82	100	82	12	3

algorithm and to determine the major and minor axes of the hair using an iterative optimisation method. Estimates for a and b and an arbitrary value of α are used initially to arrive at a theoretical value of OS′ (and thus SOS′) for the different values of β used using Equations 6 and 9. The theoretical values are then compared with the measured values. The errors are then squared, and the principle of least squares is used in order to minimise the sum of the errors by manipulating the values of a, b and α. Following iteration to minimise this sum of errors, the results are assumed to be the closest approximates for the true values of a, b and α for the hair at the given point for the number of orientations used. It was found that taking measurements of the apparent diameter at three different angles of inclination (β) gave the best compromise between effort spent and accuracy of the results. Some typical results based on simulations using true ellipses are summarised in Table I. Hence the method adopted in characterising beard hair cross-sectional area was to measure the apparent diameter at three orientations and then determine a, b and α using the Excel spreadsheet implementing the algorithm. In order to verify the accuracy of the Excel program in estimating the true cross sectional areas of real beard hair specimens, a comparison was made between the area values predicted by the Excel program and the true area, from an optical micrograph, measured using AutoCAD®. Three beard hair samples (denoted X1, X2, X3) were mounted on window cards and transverse measurements were made using an optical microscope at three specific points in each sample and at three different specimen plane orientation angles for each point. The area values at each point were calculated by using the Excel program. The samples were then mounted in methacrylate resin as shown in Fig. 1. The points at which the transverse measurements were taken were identified using a reference Tip-ex mark and images of the cross-sections at those points were taken by gradually polishing the sample embedded in the resin up to the specific point. The true areas were calculated by processing the images using AutoCAD. Table II gives a comparison of the areas at each point of the three beard hair samples. The corresponding images are shown in Fig. 8.

TABLE II Comparison of cross-sectional areas estimated from transverse measurements using the Excel program and true cross sectional areas

Sample	Point	Area from AutoCAD (μm)^2	Area from Excel (μm)^2	Error (%)
X1	1 (Fig. 8a)	12847	12899	0.4
	2 (Fig. 8b)	12343	11572	6
	3 (Fig. 8c)	11879	12758	7
X2	1 (Fig. 8d)	11006	12106	10
	2 (Fig. 8e)	13237	14958	13
	3 (Fig. 8f)	12902	13676	6
X3	1 (Fig. 8g)	17780	19557	10
	2 (Fig. 8h)	17224	21702	26
	3 (Fig. 8i)	17674	20502	16

It can be seen from the comparison that the agreements for samples X1 and X2 were reasonable. In case of sample X3, which gave a relatively high error percentage, it is to be noted that the sample cross-section was tri-lobal in shape, which is unusual. The effectiveness of the Excel program in calculating the cross-sectional area was compared against using the maximum, minimum or average measured dimensions (assuming a circular cross section). This was done by considering the measurements taken from a sample at a point at several angles and processing the cross sectional image at that point using AutoCAD to evaluate the true cross-sectional area. The results are tabulated below in Table III.

The observations clearly reveal that by using the algorithm, the error in the cross-sectional area measurement was minimised to a considerable extent.

4.2. Area variation in real beard hair samples

Using the algorithm developed for cross-sectional area characterisation, the cross sectional areas were measured for samples chosen from the three different subjects as follows.

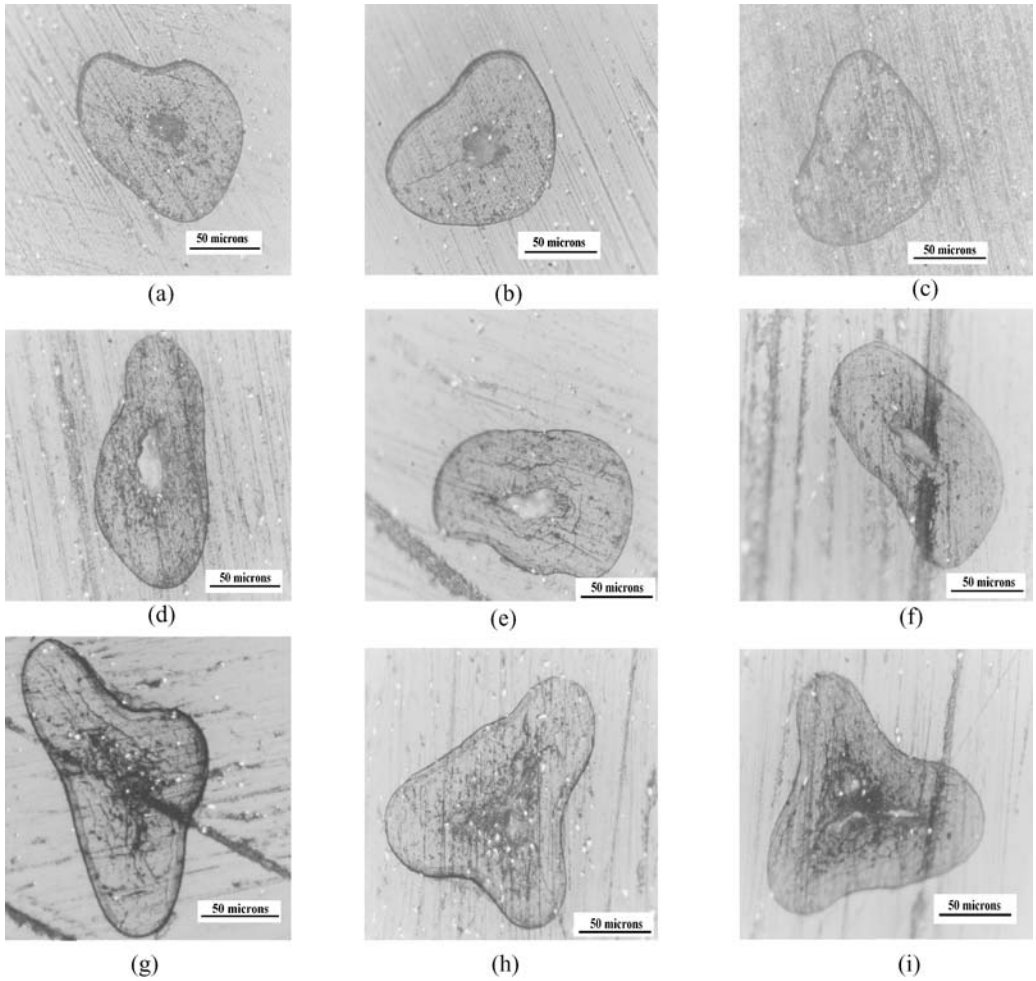

Figure 8 (a–i) Cross sectional images of samples used for checking the accuracy of the Excel program. (Samples were chosen at random from the cheeks of two different subjects from those referred to earlier).

- 40 samples from subject 'A' (20 samples taken from the cheek and 10 samples taken from the chin and the neck each).
- 20 samples from subject 'B' taken from the cheek.
- 40 samples from subject 'C' (20 samples taken from the cheek and 10 samples taken from the chin and the neck each).

For each sample, the transverse dimensions were measured at four different points along the length and at three different orientation angles per point. This led to 1200 measurements. The algorithm described in the previous section was then used to evaluate the cross-sectional area at each point. The average of the areas at the four different points was taken as the overall average cross-sectional area of the specimen. Fig. 9 shows the mean cross-sectional areas of the samples taken from the three subjects 'A', 'B' and 'C' along with the corresponding standard deviations.

Considering the measurements from the cheek over the entire range of samples, it seems that the cross-sectional area nearly doubles as we go from subject 'A' to 'C'. It is thus clear that the cross-sectional area may vary considerably from one subject to another and thus considering a wide range of the sample donors is necessary for characterising hair behaviour accurately. The standard deviations in each subset of the data indicate that the data is reasonably consistent and reliable. Within one subject, it can be

TABLE III Comparison of cross-sectional area values of a specimen calculated from four different approaches with the actual area

Actual Area (μm)^2	Angle (°)	Transverse measurements (μm)	Area (μm)^2			
			Using max. dia	Using min. dia	Using avg. dia	Using algorithm
12850	0	140	15394 (20% error)	10558 (18% error)	12337 (4% error)	12901 (0.4% error)
	45	116				
	90	120				

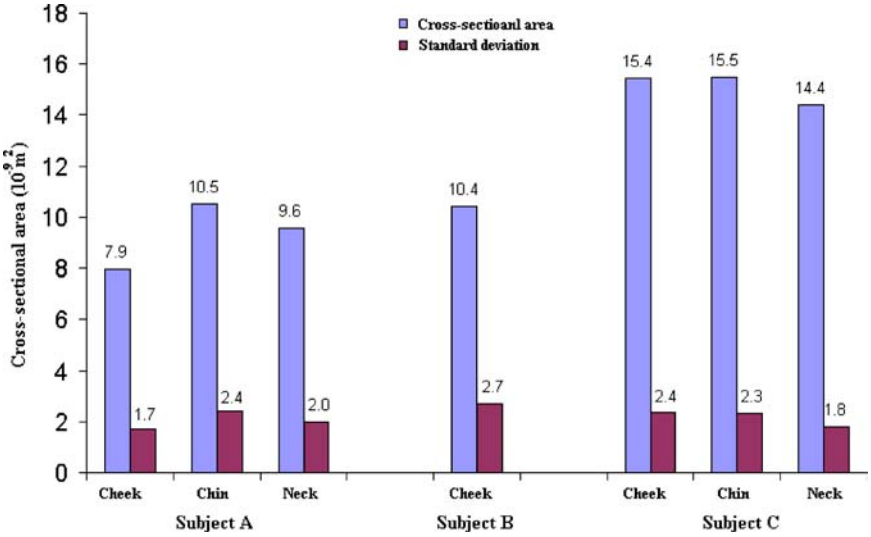

Figure 9 Overall variation of cross-sectional areas in samples taken from the three different facial sites of subjects A, B and C.

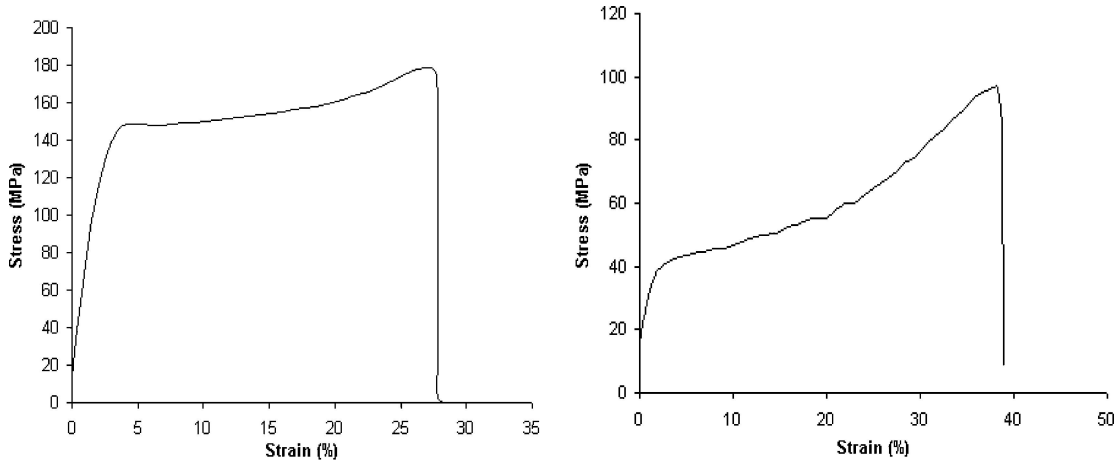

Figure 10 Typical stress strain curves for beard hair samples. Curves shown above are from two samples taken from the cheek of subject 'C' and tested at 5 mm min^{-1} in (a) dry and (b) wet condition.

seen that the variation in the cross-sectional area from one facial site to another is minor. The overall average area over the entire range of samples is about 12×10^{-9} m^2.

5. Mechanical testing

5.1. Typical tensile stress-strain behaviour

Tensile tests were performed on about beard hair samples within one and a half weeks of harvesting from the three different subjects A,B and C. Over 150 beard hair samples (chosen selectively from subjects 'A', 'B' and 'C') were tested in order to achieve a good understanding of the effect of different variables such as subject age, facial site, moisture, strain rate and ageing. Tests were carried out at three different cross-head speeds of 0.05, 5 and 50 mm min^{-1}. Tests were conducted in both dry and wet conditions. The yield stress was calculated as the 1% proof stress. Typical dry and wet stress-strain curves are shown in Fig. 10. The variation of the Young's modulus and yield stress across the range of samples tested are shown in Figs 11 and 12 respectively. The bars with solid boundaries denote the dry test results while the bars with dotted boundaries (subject C) denote the wet test results. It was found that a number of the hair samples showed slippage during the test and thus the strain to failure and failure stress could not be monitored accurately with these tests. However, it was observed that in all cases, the slippage commenced after the hair was well into the yield region. Thus it was concluded that the values of Young's modulus and yield stress quoted here are completely valid. It can be seen that there is some variation of the Young's modulus and yield stress from subject to subject. Within one subject, there is no appreciable trend of variation from site to site. The variation of Young's modulus and yield stress with strain rate are shown in Figs 13 and 14 respectively. Although the strain rate appears to be affecting the Young's modulus and yield stress to a small extent, the effect of moisture is more pronounced. It

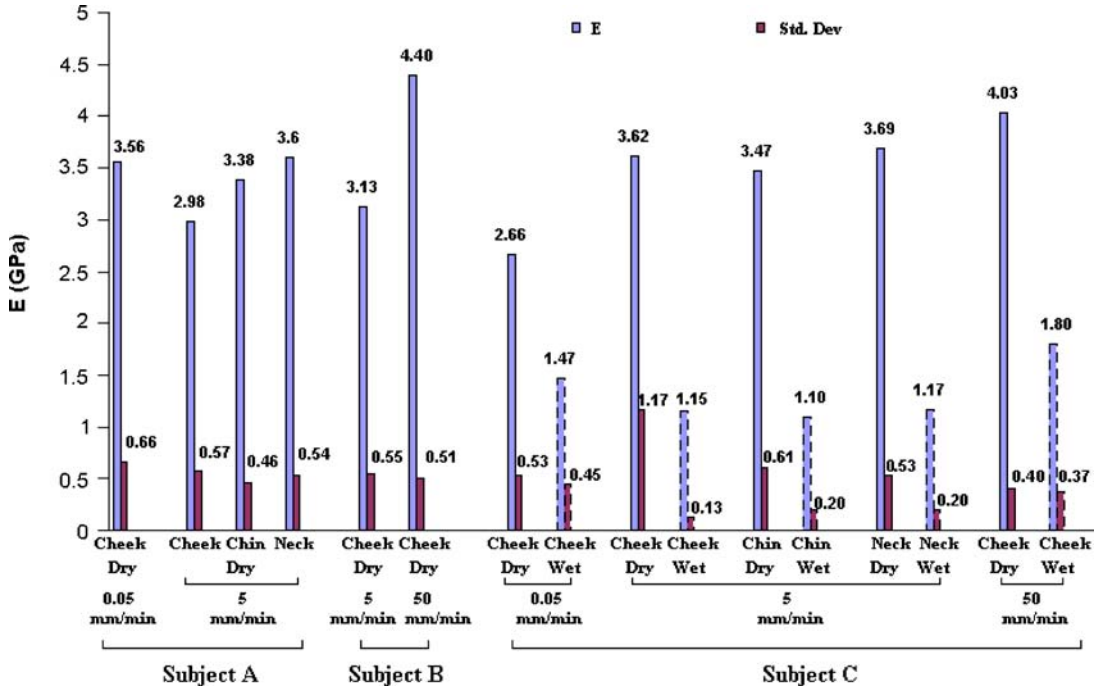

Figure 11 Variation of Young's modulus of beard hair over the entire range of samples.

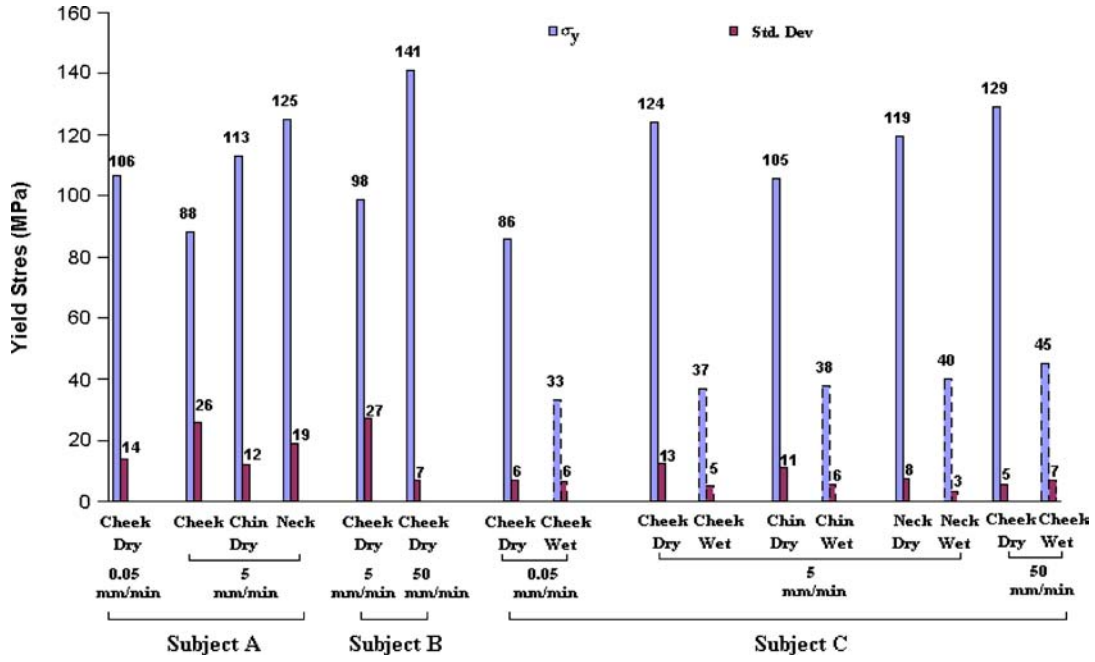

Figure 12 Variation of yield stress of beard hair over the entire range of samples.

can be seen that the value of Young's modulus and yield stress drop by almost a factor of three due to moisture (as seen in subject 'C'). It was also observed that the dry and wet ultimate tensile strength were similar, although the data has not been reported. Also, the trend of variation of Young's modulus with cross-sectional area was not consistent throughout the entire range of samples tested and thus it appears that the Young's modulus was not strictly dependent on the cross-sectional area.

Repeat tensile tests were performed on 10 samples from the cheek of subject 'C' (stored for nine months). The variation of the average Young's moduli with ageing for both wet and dry conditions are shown in Fig. 15. The variation of the corresponding yield stress values are shown in Fig. 16. There is a drop in the Young's modulus in both the wet and the dry state; the yield stress perhaps shows a decrease in the dry state but not in the wet state.

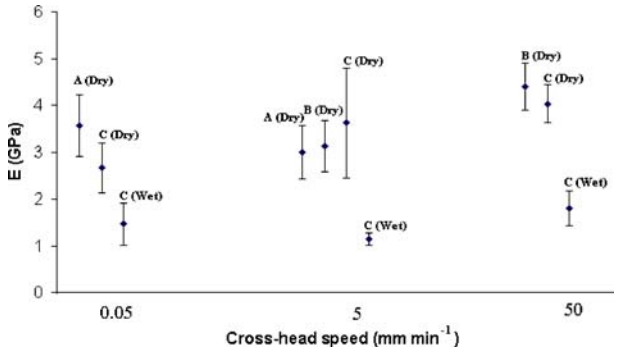

Figure 13 Variation of Young's modulus of cheek beard hair with strain rate.

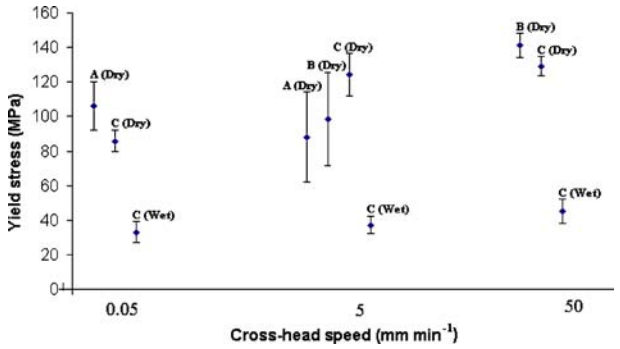

Figure 14 Variation of yield stress of cheek beard hair with strain rate.

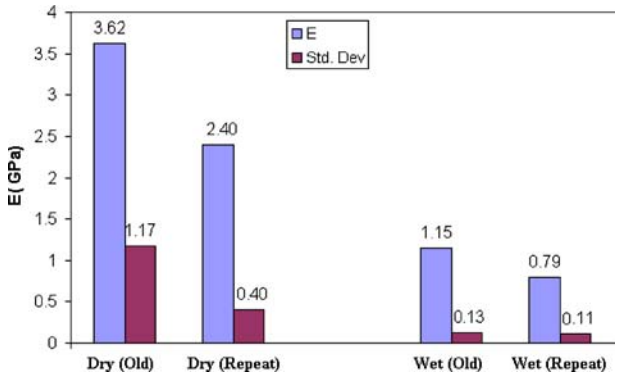

Figure 15 Variation of Young's modulus of cheek beard hair with ageing.

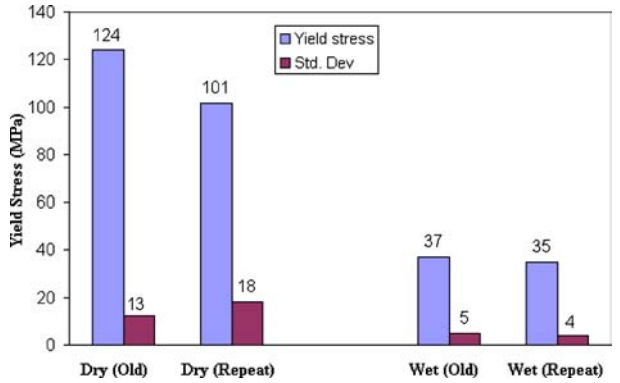

Figure 16 Variation of yield stress of cheek beard hair with ageing.

5.2. Fracture surface

Scanning electron micrographs of the fracture surfaces of typical beard hair samples that failed in tension are shown in Fig. 17. Fig. 17a shows the opposite ends of a tensile test specimen which showed gauge length failure. It can be seen from the figure that the fracture is not strictly transverse to the hair axis. Fractured units can be seen in Fig. 17b in the form of small fibrous chunks enveloped by the cuticle layers. These may be the macrofibrils (which are the major load bearing units in hair under tensile loading) or the cortical cells which are units containing 10–20 macrofibrils packed together.

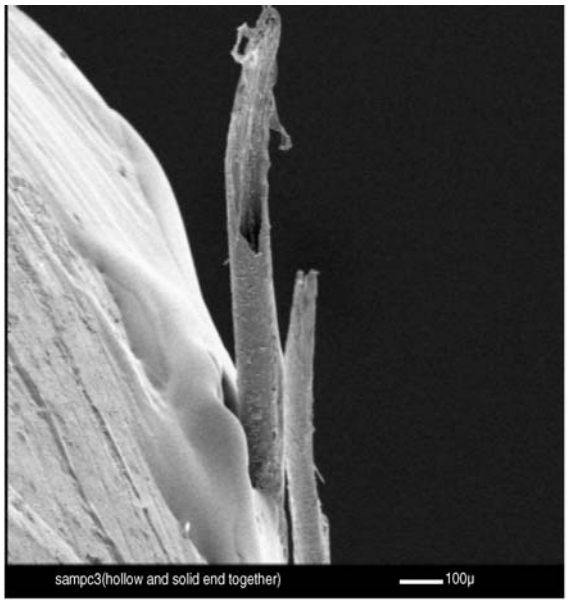

(a)

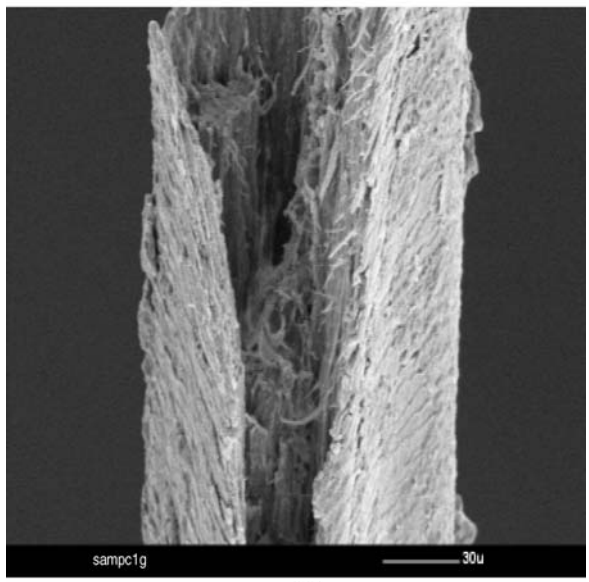

(b)

Figure 17 (a, b) Scanning electron micrographs of beard hair specimens fractured in tension.

6. Discussion

The three main regions of a typical stress-strain curve of human hair namely the elastic, yield and post-yield regions are clearly identified. The initial elastic region extends roughly up to 2–4% strain. Here the load is taken by the hydrogen bonds stabilising the alpha-helical microfibrils along with the matrix. As the hair is stretched to the yield region, the α-helices gradually transform into β-sheets and hair is no longer perfectly elastic (Astbury and Street [17], Astbury and Woods [18] as quoted by [7]). Beyond the yield region, the entire α-helix is converted into β-sheets (the transformation completes at about 50% strain and the sheet structure itself exhibits some elasticity [19]). The final phase of the stress strain curve is the post yield region where extended microfibrils take the entire load imposed on the hair before leading to complete fracture. This is the reason for the slope of the post yield curve being higher than the yield region. A series zone model was proposed [12] to explain the behaviour of hair in the yield and post yield region. According to the series zone model, hair can be assumed to consist of two alternating zones along the microfibrils namely, the X zone and the Y zone. 30% of the α-helices in the keratin are capable of exhibiting a reversible folding—unfolding nature without breaking the disulphide bonds and these form the X zone, which characterizes the yield region. Once the post yield region is reached, the remaining 70% of the α-helices unfold irreversibly by a compulsory breakdown of the disulphide bonds and they constitute the Y zone. The series zone concept was modified [13] with an extended two phase model to explain the increase of stress in the post-yield region. The model suggests that the increased stress is produced by globular matrix proteins jamming the microfibrils as the fibre is extended into the post-yield region.

It can be seen clearly from the data for subject 'C' that moisture reduces the Young's modulus and yield stress values significantly (by nearly a factor of three) regardless of strain rate value. The results are consistent with the observations with scalp hair [20]. The authors had concluded that the absorption of water by the keratin mainly weakens the matrix. Thus the contribution of the matrix to the initial stiffness is reduced thereby causing the Young's modulus and yield stresses to drop. It also appears that the Young's modulus increases with the increasing strain rate as seen in the case of subjects 'B' and 'C' although this was not seen in case of subject 'A'. Thus, it is difficult at this stage to suggest the underlying micromechanisms which determine the response of hair to different strain rates.

There appears to be some variation of values of Young's modulus and yield stress across different facial sites within one subject. However, subjects 'A' and 'C' do not show any similarity in the trend of variation from site to site. When the entire data set is analysed, there seems to be a significant degree of variation in the data and thus no significant trend is evident that is consistent for all subjects.

The values from repeat tensile tests of aged dry samples seem to suggest that there is a drop in the Young's modulus and yield stress of beard hair with time. However, in case of wet samples, the yield stress does not seem to be affected by the ageing significantly. This seems to suggest that water replenishes the hydrogen bonds stabilising the α-helices and that the bond formation is reversible. The drop in the dry Young's modulus suggests that with ageing, there is an irreversible degradation of the matrix phase, which contributes to the initial modulus in dry condition. The drop in the wet modulus could be due to the defects arising in the fibrous phase due to ageing which cannot be rectified by water intake.

7. Concluding remarks

The three main morphological features of beard hair, namely the cuticles, cortex and the medulla have been identified and characterised. Optical microscopy revealed that a majority of the beard hair samples had an elliptical type cross-section and a novel method has been developed that enables the cross-sectional area of beard hair to be determined by taking measurements at a few angles of rotation of the hair. The method is non-destructive and requires considerably less effort than sectioning and polishing. Application of the method to beard hair samples from different subjects showed that there was a significant variation in the cross-sectional area between one subject to another. However, not much variation was found between the samples taken from the different facial sites of individual subjects.

The tensile stress-strain behaviour of human beard hair shows that the general stress strain curve is similar to that observed in case of scalp hair with three distinct regions namely, the elastic, yield and post yield region. The results from the tensile tests indicate that there is a strong effect of moisture on the Young's modulus and yield stress (both being brought down nearly by a factor of 3). There appears to be some variation with facial site, subject and strain rate. However, it seems reasonable to attribute these variations to material variability since no strong trend is evident from the data. Tensile tests on aged samples revealed a significant drop in the Young's modulus in both dry and wet conditions, while the drop in the yield stress was pronounced only in the dry state.

Appendix

Algorithm for relating the transverse measurements of an elliptical prism taken under a microscope to the true major and minor diameters (the major axis being inclined to the (horizontal) measuring plane at an arbitrary angle)

Let us consider an elliptical prism, with major diameter 2a and minor diameter 2b, where the major diameter is inclined at an angle β to the (horizontal) measuring plane as shown in Fig. A.1. AA′ and BB′ are two light rays touching the ellipse at the points P and Q respectively. P′Q′ is the major axis of the ellipse which is extended

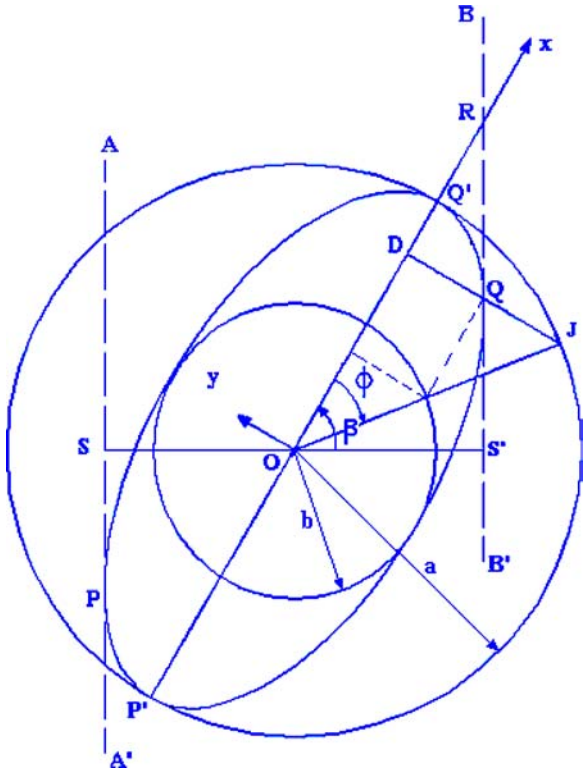

Figure A.1 Geometric representation of hair assumed to be an elliptical prism being observed under a light microscope.

to meet the ray BB′ at R such that it forms an angle '90-β' with the ray BB′. SOS′(=2 OS′) is the measured dimension in this configuration. 'Φ' is the eccentric angle for point 'Q'.

7.1. Step 1. Relate Φ to β

The co-ordinates of point

$$Q(X_Q, Y_Q) \text{ are } (a \cos \Phi, -b \sin \Phi). \tag{1}$$

with Φ defined clockwise.

It is known that the equation of a line, tangential to an ellipse at a point (X_Q, Y_Q) is

$$\frac{xX_Q}{a^2} + \frac{yY_Q}{b^2} = 1. \tag{2}$$

Substituting for X_Q and Y_Q from (1) in (2), we get

$$\frac{xa \cos \Phi}{a^2} - \frac{yb \sin \Phi}{b^2} = 1 \tag{3}$$

By re-arranging Equation 3, we get the equation of tangent BB′ in the form $y = mx+c$ where the slope 'm' is:

$$m = \frac{b}{a \tan \Phi} \tag{4}$$

Now the gradient is the tangent of the angle between BB′ and the major axis of the ellipse.

$$\text{i.e.} \quad \tan(90-\beta) = \frac{b}{a \tan \Phi} \tag{5}$$

$$\text{i.e.} \quad \frac{1}{\tan \beta} = \frac{b}{a \tan \Phi}$$

$$\text{i.e.} \quad \Phi = \tan^{-1} \frac{(b \tan \beta)}{a} \tag{6}$$

7.2. Step 2. Relate OS′ to a and b

From the figure, it can be deduced that

$$\text{OS}' = \text{RO} \cos \beta$$

$$\text{i.e.} \quad \text{OS}' = (\text{RD} + \text{DO}) \cos \beta$$

$$\text{i.e.} \quad \text{OS}' = (\text{RD} + a \cos \Phi) \cos \beta \tag{7}$$

Considering the triangle DQR in the figure, the angle DRQ $= 90-\beta$.

$$\text{Thus} \quad \tan(90-\beta) = \frac{\text{DQ}}{\text{RD}}$$

$$\text{i.e.} \quad \text{RD} = \frac{\text{DQ}}{\tan(90-\beta)}$$

$$\text{i.e.} \quad \text{RD} = \text{DQ} \tan \beta$$

$$\text{i.e.} \quad \text{RD} = b \sin \Phi \tan \beta \tag{8}$$

Substituting the expression for RD from (8) in (7), we get

$$\text{OS}' = (b \sin \Phi \tan \beta + a \cos \Phi) \cos \beta \tag{9}$$

Generally, it is not possible to start with the major axis on the (horizontal) measuring plane. It is assumed that in the initial position, the major axis is rotated by an offset angle α from the datum. In this case, β should be replaced by $\beta' = \beta + \alpha$ in the above equations where α is the initial angle of the major axis from the (horizontal) measuring plane and β' is the orientation from this initial position.

Acknowledgment

The authors would like to acknowledge the sponsorship offered by The Gillette Company to facilitate the research work discussed in this paper.

References

1. R. P. R. DAWBER, *Bioeng. Skin.* **2** (1986) 1.
2. R. DAWBER, *Clin. Dermatol.* **14** (1996) 105.
3. L. N. JONES, *ibid.* **19** (2001) 95.
4. J. A. SWIFT, *Intl. J. Cosmet. Sci.* **13** (1991) 143.
5. J. A. SWIFT, *AIM J. EXS.* **78** (1997) 149.
6. H. WATANABE and K. YAHAGI, *Jpn. J. Tribol.* **37**(4) (1992) 427.

7. M. FEUGHELMAN, *Cosmet. Sci. Technol. Ser.* **17** (1997) 1.
8. E. TOLGYESI, D. W. COBLE, F. S. FANG and E. O. KAIRINEN, *J. Soc. Cosmet. Chem.* **34** (1983) 361.
9. J. B. SPEAKMAN, *Trans Faraday Soc.* **25** (1929) 92.
10. M. FEUGHELMAN, *J. Soc. Cosmet. Chem.* **33** (1982) 385.
11. M. SAKAI, S. NAGASE, T. OKADA, N. SATOH and K. TSUJII, *Bull. Chem. Soc. Jpn.* **73** (2000) 2169.
12. M. FEUGHELMAN, *Text. Res. J.* **34** (1964) 539.
13. M. FEUGHELMAN, *ibid.* **64**(4) (1994) 236.
14. E. P. W. SAVENIJE and R. DE VOS, *Bioeng. Skin.* **2** (1986) 215.
15. C. R. ROBBINS and R. J. CRAWFORD, *J. Soc.Cosmet. Chem.* **42** (1991) 59.
16. J. A. SWIFT, *Intl. J. Cosmet. Sci.* **17** (1995) 245.
17. W. T. ASTBURY and A. STREET, *Phil. Trans. Soc. Lond.Ser. A* **230** (1931) 75.
18. W. T. ASTBURY and H. J. WOODS, *ibid.* **232** (1933) 333.
19. M. FEUGHELMAN, *J. Text. Inst.* **45** (1954).
20. J. I. CURISKIS and M. FEUGHELMAN, *Text. Res. J.* **53**(5) (1997) 271.

Received 7 May 2004
and accepted 25 May 2005